Available online at www.sciencedirect.com
SCIENCE DIRECT®
PERGAMON
International Journal of Heat and Mass Transfer 46 (2003) 1171–1181
International Journal of HEAT and MASS TRANSFER
www.elsevier.com/locate/ijhmt

Study on point of net vapor generation by neutron radiography in subcooled boiling flow along narrow rectangular channels with short heated length

M. Kureta [a,*], T. Hibiki [b], K. Mishima [b], H. Akimoto [a]

[a] Japan Atomic Energy Research Institute, Tokai Research Establishment, Tokai, Naka, Ibaraki 319-1195, Japan
[b] Research Reactor Institute, Kyoto University, Kumatori, Sennan, Osaka 590-0494, Japan

Received 14 June 2001; received in revised form 20 September 2002

Abstract

Point of net vapor generation (PNVG) was investigated based on the void fraction dataset obtained by high-frame-rate neutron radiography. The test channels used in the experiment were rectangular channels heated from one side with channel gap of 3 and 5 mm, channel width of 30 mm, and heated length of 100 mm. In this study, we discuss on (1) the determination of the instantaneous and time-averaged PNVG, (2) the effects of system parameters on PNVG, (3) the applicability of existing PNVG correlations to the channel with a short heated length, and (4) the effect of the PNVG in critical heat flux (CHF) model. The following results were obtained: (a) the effects of system parameters on the thermal equilibrium quality at the PNVG were small under the present conditions, (b) existing PNVG correlations tended to underestimate the thermal equilibrium quality at the PNVG in the channel with a short heated length, and (c) the prediction accuracy of Katto's CHF model could be improved significantly by using the accurate PNVG.

1. Introduction

In relation to thermal-hydraulic design of high heat flux components, it is important to predict a critical heat flux (CHF) in a cooling channel with a relatively short heated length. Some experimental [1] and analytical [2–4] researches have been performed on the CHF in round tubes with a short heated length. On the other hand, cooling channels in high intensity spallation neutron source (SNS) and fusion neutron source (FNS) being planned in the Japan Atomic Energy Research Institute (JAERI) have a rectangular cross section and a relatively short heated length of about 100 mm. The applicability of existing CHF correlations and models, which were developed based on the dataset mainly taken in round tubes, to such a rectangular channel with a short heated length should be evaluated by database taken for appropriate channel geometries. The present authors performed experimental work to collect rigorous database of the CHF in rectangular channels with a short heated length under subcooled-boiling conditions as well as analytical work to evaluate existing CHF correlations and models with the obtained database [5,6]. This preliminary analysis suggested that the correlation for void fraction employed in the CHF model did not give a good prediction for the short rectangular channels, resulting in marked deterioration of the accuracy in the CHF prediction.

For good prediction of the void fraction in a subcooled-boiling region, a proper modeling is indispensable for the point of net vapor generation (PNVG), the true quality (x), and the void fraction distribution. Among them, the prediction of the PNVG may affect the calculated void fraction distribution at the downstream from the PNVG significantly. Thus, a physical understanding of the PNVG is indispensable to predict the void fraction with high accuracy. Different CHF models give different PNVG definitions, such as the net vapor

* Corresponding author. Tel.: +81-29-282-6428; fax: +81-29-282-6427.
E-mail address: kureta@hflwing.tokai.jaeri.go.jp (M. Kureta).

0017-9310/03/$ - see front matter © 2002 Elsevier Science Ltd. All rights reserved.
PII: S0017-9310(02)00398-8

Nomenclature

d	transverse position (m)
D_e	hydraulic equivalent diameter (m)
F_{PNVG}	normalized value of the instantaneous point of net vapor generation (–)
G	mass velocity ($kg\,m^{-2}\,s^{-1}$)
L_h	heated length (m)
q	heat flux ($W\,m^{-2}$)
s	channel gap (m)
t	thickness (m)
T_{in}	inlet water temperature (°C)
ΔT	measurement time (s)
w	channel width (m)
w_h	width of the heated surface (m)
x	true vapor quality, dimensionless (–)
x_d	equilibrium vapor quality at the point of net vapor generation (–)
x_{eq}	equilibrium vapor quality (–)
x_{ex}	equilibrium vapor quality at the exit of the heated section (–)
x_{in}	equilibrium vapor quality at the inlet of the heated section (–)
z	flow-directional distance from the heated inlet (m)
z_d	flow-directional distance from the heated inlet to the point of net vapor generation (m)

Greek symbol

α	gap-wise averaged local void fraction (–)

Subscripts

CHF	critical heat flux
ex	exit conditions
f	liquid single phase
g	gas single phase
HA	heated-area averaged
i	instantaneous value
$\langle\ \rangle$	value averaged over the cross-sectional area

generation point (NVGP), the initial point of net vapor generation (IPNVG), onset of significant void (OSV). The definition of the PNVG would roughly be classified into two types. Levy [7] and Saha–Zuber [8] defined the PNVG to be a point where bubble departure from the channel wall initiated, whereas Bibeau–Salcudean [9] defined it to be a point where the net void fraction started to increase. The present authors found from high-speed-video visualization of subcooled-boiling flow in a rectangular channel heated from one side [5] that the bubble migration on the heated surface occurred even at the upstream of the point of net void fraction increase. Similar observation was also reported by Dix [10] in an experiment at a high pressure. Therefore, it should be important to discriminate between the definitions of the PNVG by Levy and Saha–Zuber and by Bibeau–Salcudean. The definition of the PNVG in this study follows the latter.

In relation to the thermal-hydraulic design of the cooling channels in the MTR-type research reactor, much works have been done for void fraction measurement in narrow-rectangular channels. Egen et al. [11], and Maurer et al. [12] measured void fraction in rectangular channels with a few millimeters gap by γ-ray transmission method and Staub et al. [13], and Martin et al. [14] by X-ray transmission method. These data have often been used for evaluating CHF models in forced convective boiling flows. However, the length of the channels used in their experiments was about 350 mm or longer, and the dataset only provided time-averaged void fractions at a single measurement point or traversed measurement points.

In this study, void fraction in a rectangular channel heated from one side was measured by high-frame-rate neutron radiography (HFR-NR). Neutron radiography (NR) is one of non-intrusive measurement techniques, which make use of the difference in attenuation characteristics of neutrons in materials. In comparison with other non-intrusive methods like X-ray radiography, NR is suitable for measurement of thin water-thickness on the order of a few millimeters. The details of the NR imaging technique were described in the previous paper [15]. The purpose of this study is to obtain the PNVG from instantaneous (temporal resolution: 0.89 ms) and time-averaged void fraction data measured using HFR-NR. In addition, the applicability of existing correlations for PNVG to a rectangular channel with a short heated length was examined, and the effect of the PNVG estimation on the prediction accuracy of Katto's CHF model was evaluated.

2. Experimental apparatus

An experimental system consisting of a test section, water-circulation loop, a direct current power supply for joule heating, and a high-speed video system was installed in a thermal neutron radiography facility no. 2 (TNRF-2) at the JRR-3M research reactor of the JAERI. The basic concept and imaging procedure of

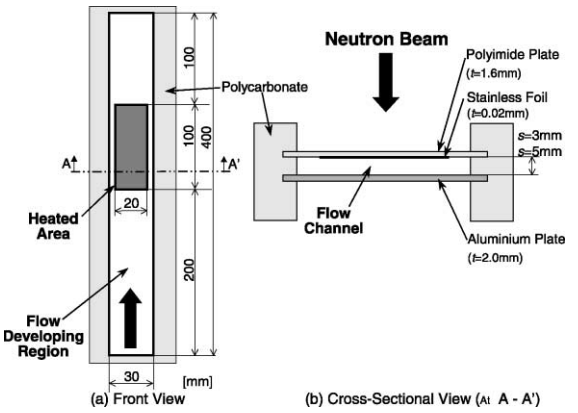

Fig. 1. Schematic view of the test section.

HFR-NR, and the estimation of the measurement error were detailed in the previous paper [15].

Fig. 1 shows the schematic diagram of the test section. The test sections were rectangular channels heated from one side with channel gaps, s, of 3.0 and 5.0 mm. The channel width, w, width of the heated surface, w_h and heated length, L_h were, 30, 20, and 100 mm, respectively. One side of the channel wall was a polyimide plate with vapor-deposited 20 μm thick stainless steel foil, whereas another side was an aluminum plate. The dimensions of the flow channels were determined based on the conceptual design parameters of a rotating target of the FNS and a solid target of the SNS being planned in the JAERI. Thus, the obtained data will be utilized to develop a CHF model for a rectangular channel with a short heated length and a small gap in the target systems. The length of entrance region for stabilizing a flow and the non-heated width on both sides of the heated surface were determined from the velocity distribution of a single-phase flow calculated by ACE-3D computational code [16], which adopted $k-\varepsilon$ model for turbulent calculation. This calculation estimated that the velocity distribution at the inlet of the heated section was fully-developed for water single-phase flow and the span-wise velocity distribution was almost flat in the heated width.

The working fluid was ion-exchanged water, and the temperature was controlled to keep a preset value at the inlet. The flow rate was measured by an orifice flow meter. A constant flow rate was kept by preventing the decrease in the flow rate caused by the increase in the pressure loss in the test section due to boiling. The test section was placed in the TNRF-2 so that the flow direction was vertically upward. A vapor–water separator installed at the top of the test section was connected with the atmosphere and, thus, the pressure at the exit of the test section was maintained at the atmospheric pressure. The stainless steel foil was uniformly joule-heated by a direct-current power supply unit (300 A–60 V) through copper electrodes.

The water temperature at the inlet, T_{in} ranged from 70 to 90 °C, and was kept constant within ±0.1 °C. The mass velocity, G, ranged from 240 to 2000 kg/(m^2 s), and was kept constant within ±5% relative deviation. Insulating materials were removed from the visualization and measurement area in the test section to avoid the neutron absorption in the insulating materials. Total heat loss in the test section was estimated by heat balance calculation to be 2% of the total heat input.

Two experimental procedures were adopted as (1) heat flux was increased stepwise to a CHF at constant mass velocity and inlet subcooling, and (2) mass velocity was decreased stepwise to a CHF at constant heat flux and inlet subcooling. In each step, after a flow reached to be stable, NR images were recorded. The increment of the heat flux was set at a few % or less than the preset value around the CHF, and images of the boiling flow were recorded until just before CHF.

The HFR-NR imaging system consisted of a neutron-visible light converter, an image-intensifier, and a high-speed video system (Fast-cum Ultima, Photron) with a spatial resolution of 300 ~ 600 μm/pixel). The recording speed in the experiment was set at 1125 frames/s ($\Delta T = 0.89$ ms). Since the image blur due to rapid bubble movement may have affected only 1 or 2 pixels, such a recording speed would be sufficient to visualize the behavior of moving steam bubbles. The measurement error of instantaneous void fraction ($\Delta T =$ 0.89 m s) was estimated to be within ±18% [15].

3. Experimental results

3.1. Instantaneous void fraction

Temporal variation of spatial distribution of local instantaneous void fraction was obtained as sequence images taken every $\Delta T = 0.89$ m s. Fig. 2 shows an example of the temporal variation of spatial distribution of local instantaneous void fraction in subcooled boiling flow measured just before CHF. The experimental condition was $s = 5$ mm, $G = 600$ kg/m^2 s, $T_{in} = 90$ °C, and $q = 0.9$ MW/m^2 ($q/q_{CHF} = 0.99$). It should be noted here that the local void fraction means the gap-wise averaged void fraction. HFR-NR could successfully measure a two-dimensional void fraction distribution in a narrow channel with high temporal-resolution without disturbing flow, which might hardly be measured by other methods. Time-series data of the local instantaneous void fractions stored in a computer were reconstructed as two-or three- dimensional pseudo-colored images. Then, the flow behavior of steam bubbles was observed by temporal and spatial variations of the void fraction in the animated images. Although the total flow

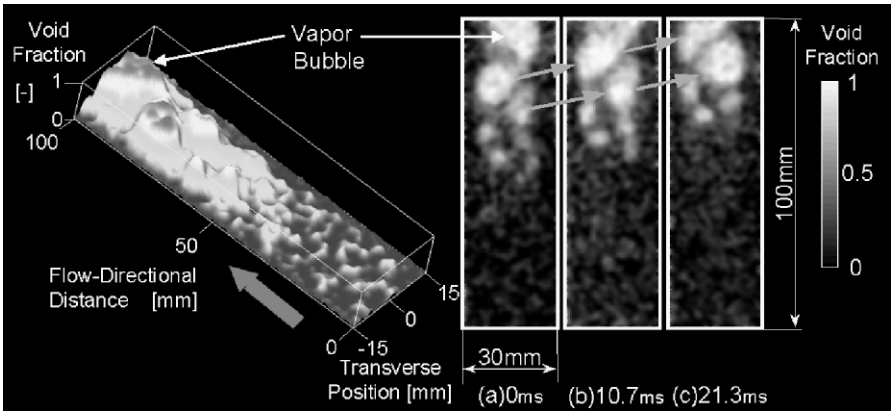

Fig. 2. Instantaneous void fraction distribution images.

rate at the inlet was kept constant, the flow regime was periodically changed for the condition of high void fraction at the exit. The point at which the local void fraction started to increase (PNVG) remarkably was also fluctuated. Such a periodical variation significantly affected the local instantaneous void fraction at the exit where the CHF occurred. Particularly, the periodical fluctuation of the PNVG affected the change rate of the local instantaneous void fraction at the downstream of the PNVG markedly. Since the mechanism of the PNVG fluctuation would be thought to be important to understand the flow characteristics at CHF, further detailed analysis was performed as follows. To determine the PNVG from the animated image of the local instantaneous void fraction, the image processing was performed by reversing the local instantaneous void fraction in terms of the time. In the image processing program, a steam bubble was traced back to the past where a steam bubble returned to the PNVG. The PNVG was determined to be a point where the maximum local void fraction of the traced bubble reduced below the value of sum of the cross-sectional averaged void fraction and its standard deviation. In what follows, the point obtained by the above procedure was described as the PNVG.

3.2. Instantaneous PNVG

Fig. 3 shows an example of instantaneous PNVG distribution measured in the same experimental condition as that in Fig. 2. The ordinate in Fig. 3 indicates the normalized values of the instantaneous PNVG frequency. When a bubble starts to grow around the inlet ($z = 0$ mm), the value in the lower right in Fig. 3 takes high value. The instantaneous PNVG distribution in Fig. 3 was obtained from 2250 instantaneous void fraction data, corresponding to 2 s in real time. Since it was difficult to measure simultaneously two-dimensional

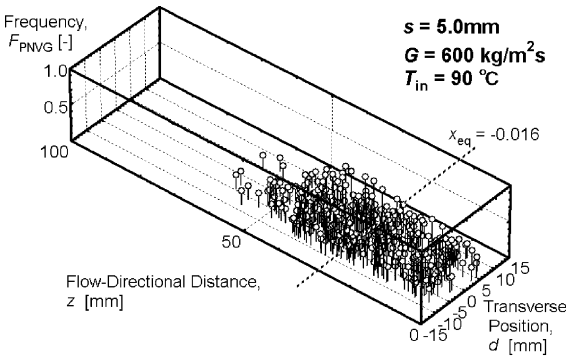

Fig. 3. Instantaneous PNVG distribution.

void fraction distribution by other methods, it was necessary to use NR to determine the instantaneous PNVG from measured instantaneous two-dimensional void fraction distribution. It can be understood from Fig. 3 that periodical variation of the flow (the period was about 25 m s for the conditions in Figs. 2 and 3) caused the fluctuation of the instantaneous PNVG over the range from $z = 0$ to 60 mm. In Fig. 3, the dotted line indicated by "$x_{eq} = -0.016$" represents thermal equilibrium quality at the time-averaged PNVG as described later. The instantaneous PNVG moved around the time-averaged PNVG within the distance of ± 30 mm, corresponding to the change in thermal equilibrium quality of ± 0.002. The fluctuation was relatively small for low void fraction, i.e., the flow with small bubbles. It was thought that the fluctuation of bubble characteristics such as size and velocity, was strongly affected by the balance between the evaporation and condensation under subcooled flow conditions. To predict the CHF based on the phenomena, numerical analysis code that can calculate the interfacial heat transfer, interfacial area concentration and two-phase turbulent flow etc. with

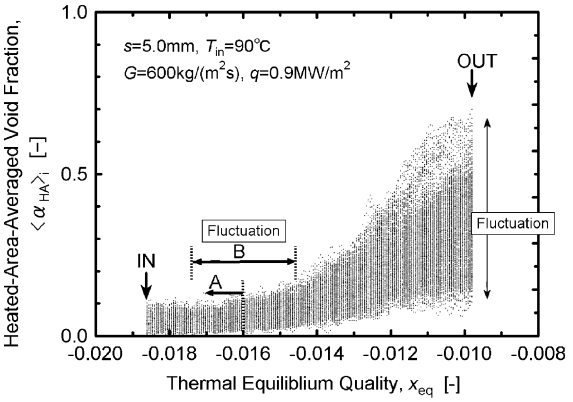

Fig. 4. Fluctuation of instantaneous void fraction.

high accuracy should be developed. In Fig. 4, the instantaneous heated-area averaged void fraction, $\langle\alpha_{HA}\rangle_i$ is plotted as the thermal equilibrium quality, x_{eq} along the flow direction. Here, the heated-area averaged void fraction refers to the averaged void fraction in the projected area as (heated width) × (channel gap). The heated-area averaged void fraction is defined here to be used for future evaluation of existing CHF models, since averaged steam-layer thickness over the heated surface at CHF can roughly be estimated by $\langle\alpha_{HA}\rangle_i \times s$.

Preliminary observation indicated that in the channel with the short heated-length, vapor bubbles at increased heat fluxes were generated even at the inlet [5]. Under the condition shown in Fig. 2, the instantaneous void fraction began to fluctuate from near the inlet as indicated by region A in Fig. 4. In this experimental condition of short-heated length and high heat flux, it is thought that the wall voidage region started near the inlet. It should be noted here that Fig. 4 shows the fluctuation of local void fraction, $\langle\alpha_{HA}\rangle_i$ for 1 s and region B also indicates the range within the standard deviation of the fluctuation of the instantaneous PNVG. The moment at which the instantaneous PNVG reached the upstream end of region B may correspond to the condition when the liquid flow rate momentarily decreased due to the periodic variation of the pressure drop in the channel. Bubbles, which started to grow near the inlet, tended to coalesce and expand along the flow direction. In other words, bubbles with high instantaneous void fraction at the exit were possibly those which started to grow near the inlet. To model CHF process in a channel with a short heated length, special attentions should be paid to the following observation: the instantaneous PNVG would possibly fluctuate over half of the channel length, and (b) the instantaneous void fraction at the exit, and so the vapor layer thickness, would change remarkably. It was observed in the previous experiments [5] that CHF occurred when a bubble with a maximum length passed through the exit and caused a thin liquid film dryout during its passage time.

Under the flow condition indicated in Fig. 2, the exit quality, x_{ex} was −0.01 which is very close to zero. Since it is thought that subcooled water was flowing along the non-heated sections beside the heated section, the local flow regime in the heated section near the exit would presumably be a saturated boiling. In this study, the similar image processing was also conducted for the experimental data taken in the flow conditions of $G < 2000$ kg/(m^2 s) and $T_{in} > 80$ °C. Since the flow condition indicated in Fig. 2 was a subcooled boiling flow very close to saturated boiling, considerable bubble coalescence and expansion were observed. On the other hand, for a higher mass flow rate and lower inlet water temperature, the shrinkage of bubbles due to vapor condensation, which is a typical bubble behavior in subcooled boiling flow, was observed.

It was found from this study that the instantaneous PNVG fluctuates around the time-averaged PNVG and its deviation strongly depends on the flow conditions. At the moment, however, it is thought to be difficult to predict the instantaneous void fraction and CHF by using the instantaneous properties, because almost all the computer codes now available employ correlations which have been developed in terms of statistically averaged properties. This should be a subject for further study. On the other hand, existing prediction methods for void fraction and CHF have been developed in terms of statistically averaged properties. Time averaged PNVG and void fraction will then be presented in the following sections for verifying those correlations based on the present experimental results.

3.3. Time-averaged void fraction

The time-averaged void fraction and its standard deviation were calculated from the measured instantaneous void fraction. For a flow with small temporal-variation of the void fraction like an annular flow, it is possible to measure time-averaged void fraction with high accuracy by means of even an imaging system with low temporal-resolution. However, for a flow with large temporal-variation of the void fraction like a slug flow (see Fig. 2), the time-averaged void fraction should be obtained by averaging the measured instantaneous void fraction over time; otherwise the measurement error might be increased. Since HFR-NR was used in this study, the time-averaged void fraction could be measured accurately within the error of ±2% [15]. Taking the periodicity of flow variation into account, the time-averaged void fraction was calculated from averaging the instantaneous void fraction over 2 s (2250 images). Fig. 5 shows the time-averaged void fraction for the flow condition indicated in Fig. 2. Each black point in the figure represents a measured point. From the

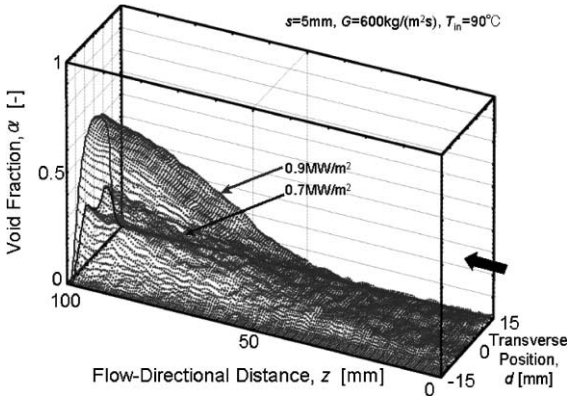

Fig. 5. Time-averaged void fraction distribution.

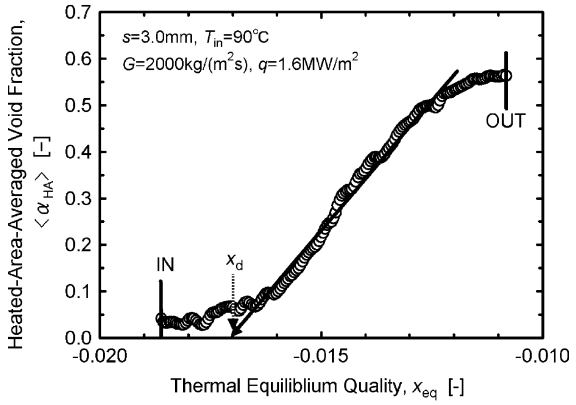

Fig. 6. Determination of thermal equilibrium quality at the PNVG x_d by the least square estimation.

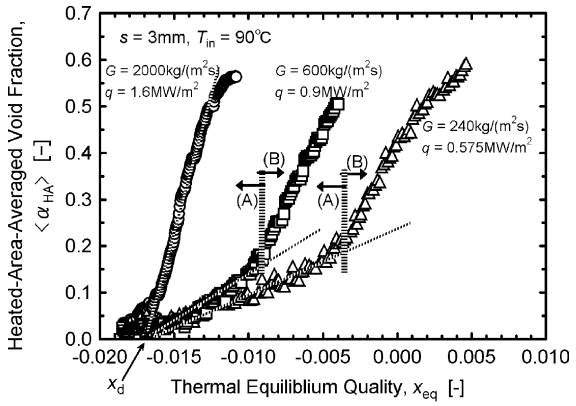

Fig. 7. Determination of thermal equilibrium quality at the PNVG x_d by the least square estimation.

comparison of the time-averaged void fraction distribution and the time series of the instantaneous local void fraction distributions at the same flow condition, important flow characteristics were clarified as follows. (1) As shown in Fig. 5, the change in the transversal void fraction profile at the exit with changing the heat flux was caused by the phenomena that vapor bubbles generated at the side edges of the heated section expanded towards the channel center and coalesced. (2) As shown in Figs. 2 and 5, the instantaneous local void fraction at the exit where the CHF occurred varied around the time-averaged void fraction as much as $\pm 30\%$. (3) The time-averaged void fraction gradually increased along the flow direction. However, the observation of bubbles growing along the flow direction by sequential instantaneous local void fraction data revealed that a bubble cluster with a vapor layer twice the time-averaged thickness flowed upward with changing the bubble density.

3.4. Time-averaged PNVG

Different researchers have employed different determination methods of time-averaged PNVG. In this study, the time-averaged PNVG was determined by a linear extrapolation of the heated area averaged void fraction profile, which was approximately in linear proportion to the thermal equilibrium quality just at the downstream of the point where net bubble growth started (see Fig. 6). In Fig. 3, the dotted line indicated by "$x_d = -0.016$" corresponds to the thermal equilibrium quality, x_d at the time-averaged PNVG. It was confirmed that the time-averaged PNVG determined by the linear extrapolation was close to the averaged value of instantaneous PNVG. Fig. 7 shows the heated area averaged void fraction as a function of the thermal equilibrium quality near the CHF condition for a low mass velocity. Similar dependence of $\langle \alpha_{HA} \rangle$ on x_{eq} as shown in Fig. 6 was observed in various flow conditions. However, for the low mass velocity and low quality close to 0, steep changes in the slope were observed between regions A and B as shown in Fig. 7. Egen et al. [11] reported the similar dependence of $\langle \alpha_{HA} \rangle$ on x_{eq} in their experiment using a channel heated from both sides ($w_h = 25.4$ mm, $s = 2.6$ mm, $L_h = 685.8$ mm). Thus, it was found for a low flow rate in a rectangular channel that the void fraction was increased markedly in region B after gradual increase of the void fraction in region A. In order to investigate the cause of such a rapid slope-change, a time-series of instantaneous void fraction distributions was observed with special attention of the point where the slope was steeply changed. The observation recognized that marked expansion of vapor bubbles and bubble coalescence in the spanwise direction were initiated near the point. Even for the same high void fraction conditions, the variation of the instantaneous void fraction depended on the mass veloc-

ity. As the mass velocity increased, the condensation effect of subcooled water flowing in non-heated sections was likely to become significant. Since vapor condensation was observed in region A, the boiling regime was thought to be pseudo-saturated boiling flow. On the other hand, since no vapor condensation was observed in region B, the boiling regime was considered to be local saturated boiling flow. The major difference between the boiling regimes for high mass flow rate (see data for $G = 2000$ kg/m^2 s in Fig. 7) and low mass flow rate (see data for $G = 240$ and 600 kg/m^2 s) is as follows. For high mass flow rate, vapor condensation at the exit occurred even under high heat flux and high void fraction conditions (region A), whereas for low mass flow rate, saturated boiling occurred locally at the exit (region B).

Since the averaged void fraction reached to about 0.15 in the region A and the bubble growth started at low quality condition in region A, the time-averaged PNVG was determined by using the data taken in region A (see dotted line in Fig. 7).

3.4.1. Effects of heat flux and channel gap on PNVG

Fig. 8 shows the dependence of x_d on the heat flux at $T_{in} = 90$ °C with the channel gap, s, and mass velocity, G as parameters. The dotted line in the figure indicates the thermal equilibrium quality at the inlet, x_{in} and the error bars represent the standard deviation of the variation of the quality at instantaneous PNVG. The thermal equilibrium qualities at the exit were dependent on s and G. Effects of heat flux and channel gap on x_d were found to be small in the tested experimental conditions.

3.4.2. Effect of mass velocity on PNVG

The effect of mass velocity on x_d was discussed based on the data obtained by decreasing stepwise the mass velocity at constant heat flux and inlet water temperature. Fig. 9 shows an example of the results with the heat flux as a parameter. From Figs. 8 and 9, it can be seen that the effect of mass velocity on x_d was not marked. Such insignificant effects of heat flux and mass velocity on x_d could also be explained by the fact that x_d-data taken under three different conditions almost coincided in values (see lower left in Fig. 7).

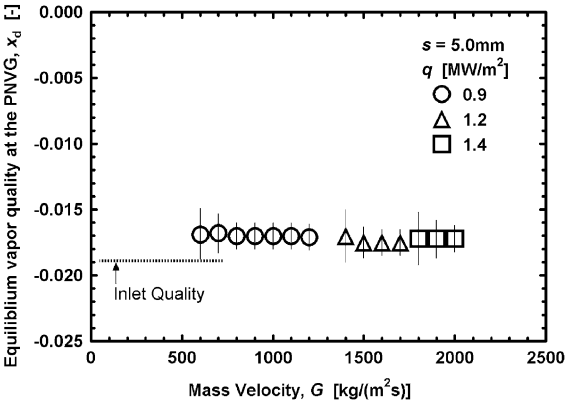

Fig. 9. Effects of mass velocity on the PNVG.

3.4.3. Effect of inlet velocity on PNVG

Figs. 10 and 11 show the effect of the inlet water temperature on x_d Fig. 10 shows the variation of the heated-averaged void fraction along the flow direction with the inlet water temperature as a parameter. The difference in void fractions measured for $T_{in} = 80$ and 85 °C was small, and the void fraction started to increase at the thermal equilibrium quality indicated by dotted box in Fig. 10 in the tested temperature range (80 °C $\leqslant T_{in} \leqslant$ 90 °C). It was difficult to measure the void fraction at $T_{in} < 80$ °C because of low void fraction (<0.1), and at $T_{in} > 90$ °C because of unstable flow. As the inlet water temperature was decreased, the thermal equilibrium quality at the inlet was lowered as indicated by the

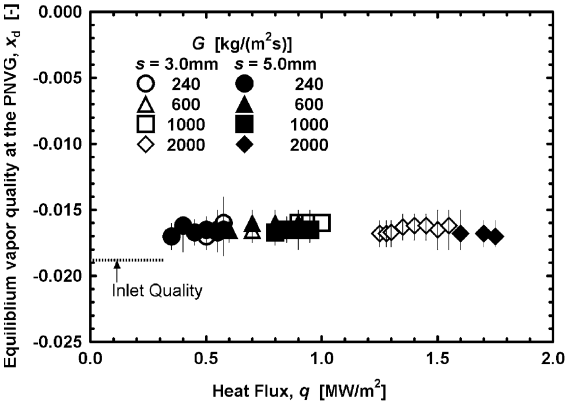

Fig. 8. Effects of heat flux and channel gap on the PNVG.

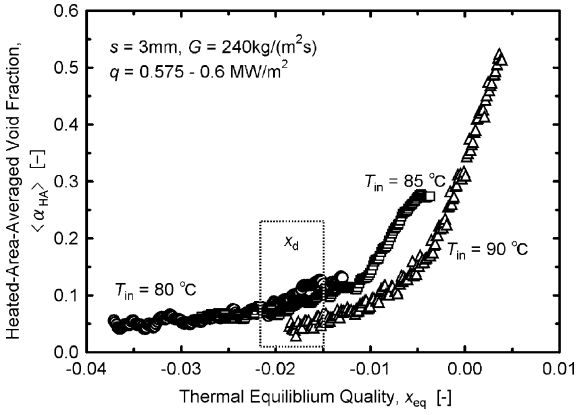

Fig. 10. Effects of inlet water temperature on the PNVG.

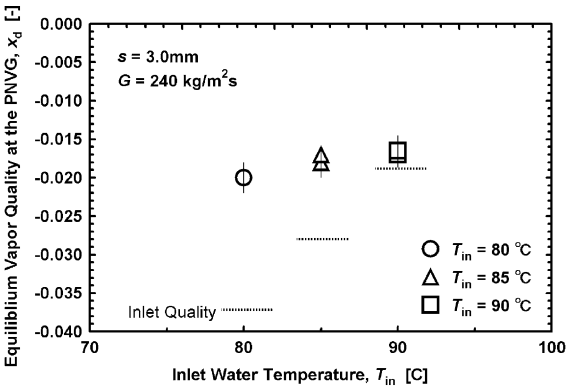

Fig. 11. Effects of inlet water temperature on the PNVG.

dotted lines in Fig. 11. Although the water temperature at the inlet would affect the void fraction distribution significantly, the effect of the water temperature on x_d was small.

It could be concluded from measured x_d in the channels with a short heated length that the influence of system parameters on x_d was small. The averaged value of x_d in the tested conditions was −0.0165. In what follows, the PNVG of boiling flow in a channel with a short heated length is discussed from the comparison of the measured PNVG and existing correlations.

4. Discussions

4.1. Comparison of existing PNVG correlations and experimental results

PNVG correlations proposed by Levy [7], Saha–Zuber [8], and Bowring [17] were compared with the experimental results. As described in Introduction, the PNVG in their correlations was defined as a point where bubbles started to depart from the wall, whereas the PNVG in this study was defined as a point where void fraction started to increase significantly. It was observed [5] that the bubbles already started to migrate at the upstream of the PNVG defined in this study. Thus, due to the different definition of the PNVG, it is expected that the existing correlations under-predict the PNVG defined in the present study. Fig. 12 shows the com-

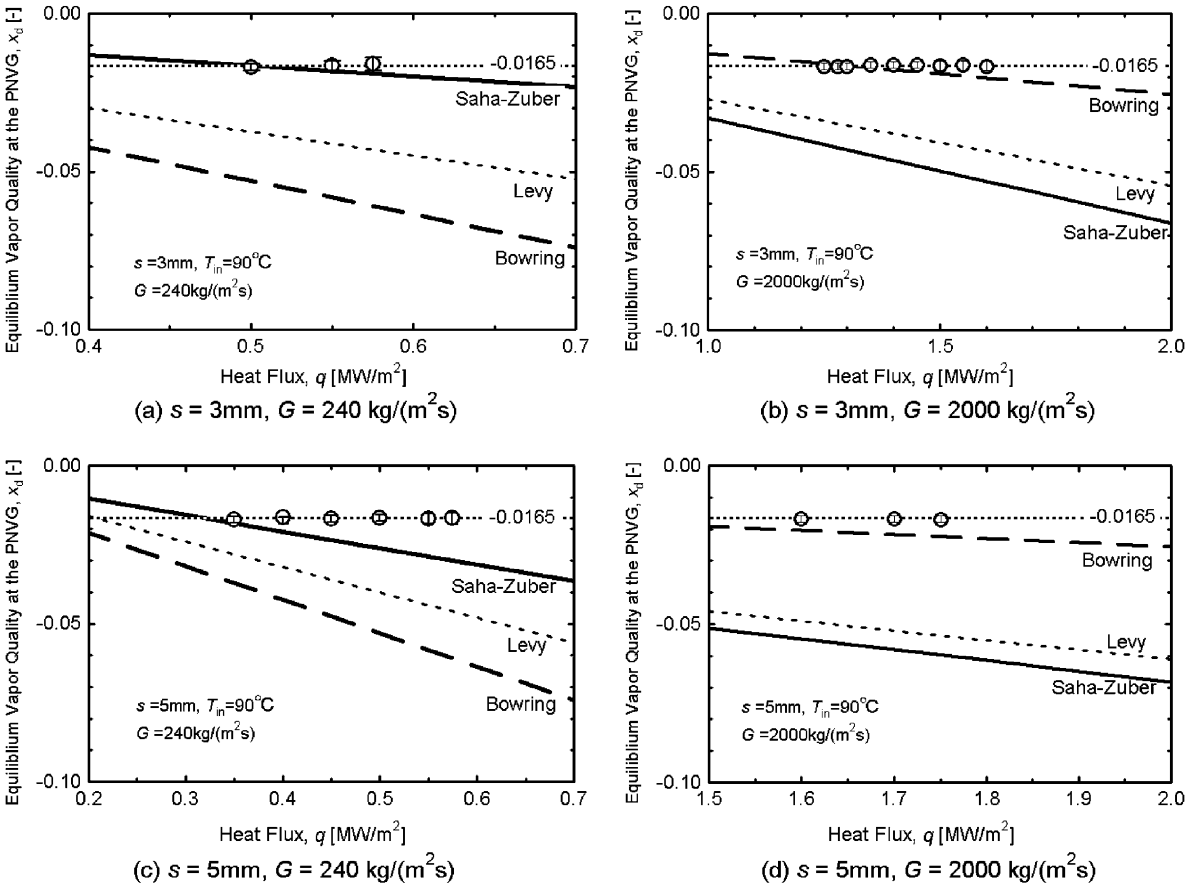

Fig. 12. Comparison of the PNVG with exiting PNVG equations.

parison of measured x_d and the predictions by the existing correlations. In Fig. 12, (a) and (b) are the results for $s = 3$ mm and (c) and (d) are the results for $s = 5$ mm, whereas (a) and (c) are the results for $G = 240$ kg/m^2 s and (b) and (d) are the results for $G = 2000$ kg/m^2 s. The inlet water temperature and the inlet quality, x_{in} were 90 °C, and −0.0187, respectively. The dotted lines through the data points indicate the arithmetic averaged value of measured values to be −0.0165. For the low mass velocity, Saha–Zuber's correlation among the correlations gave predictions closest to measured x_d whereas for the high mass velocity, it underestimated the measured values. On the other hand, x_d predicted by Bowring's correlation increased with increasing mass velocity, and the prediction for $G = 2000$ kg/m^2 s was closest to the measured values in comparison with predictions by other correlations. Table 1 shows the flow conditions where each correlation could be applied and those in the present experiment. As indicated in Table 1, Levy's and Saha–Zuber's correlations were developed based on the data taken under relatively low mass velocity conditions. On the other hand, Bowring's correlation was tested for the mass velocity up to 2000 kg/m^2 s, which is the same as the present experiment, although the pressure range is much higher than the present experimental condition. The underestimations by Saha–Zuber's correlation at a high mass velocity and by Bowring's correlation at a low mass velocity would be attributed to the different definition of PNVG and the application of the correlations over the applicable limit of the flow range. The test sections used in the present experiment were rectangular channels heated from one-side ($D_e = 5.5$ mm and 8.6 mm, $L_h = 100$ mm), whereas the data base used for developing the existing correlations were collected in round tubes, annuli, and rectangular ducts ($D_e = 4.0$ mm ~ 24 mm, $L_h =$ 346 mm $\sim$ 1524 mm). The major difference between the present experimental condition and the applicable range of the existing correlations would be heated length. In this study, the heated length, L_h was relatively short to be 100 mm in comparison with the applicable rage of the existing correlations. Most of the PNVG in the database existed in the thermally developed region, whereas in the present experiment, the marked increase in the void fraction started in the thermally developing region. For such a channel with a short heated length where the PNVG existed in the thermally developing region, the existing PNVG correlations predicted that bubble departure from a wall and steep increase in the void fraction would occur at the inlet. However, experimental results indicated that the bubble departure from a wall and the steep increase in the void fraction did not occur at the inlet, and that the PNVG depended on the experimental conditions. For evaluating the effect of the PNVG in the CHF models, PNVG correlation for present conditions was requested. In the tested conditions, $x_d = -0.0165$ could give a good prediction of the PNVG.

In a future work, a mechanistic model and a numerical simulation method to predict PNVG should be developed for a channel with a short heated length where steep increase in the void fraction is initiated in the thermally developing region, and non-circular channels like a rectangular channel in which the effect of the thermal non-equilibrium on the void fraction distribution is significant.

4.2. Evaluation of PNVG and prediction of CHF in rectangular channel heated from one side

Effect of the prediction accuracy of PNVG on the predictions of CHF and void fraction is examined in this section. For the CHF condition indicated in Fig. 2, the CHF model proposed by Katto [18] predicted 4.2 times higher CHF than the measured one, namely $C/E = 4.2$, where C/E refers to the ratio of predicted CHF value to experimental value. In the Katto's model, the equilibrium quality at the PNVG x_d the true quality x, and the void fraction were determined by Saha–Zuber's correlation, the profile-fit method and the homogeneous equilibrium mixture model, respectively. The profile-fit method used in Katto's model is expressed by the following equation:

$$x = \frac{x_{eq} - x_d \cdot \exp\left(x_{eq}/x_d - 1\right)}{1 - x_d \cdot \exp\left(x_{eq}/x_d - 1\right)} \quad \text{for } x_d < x_{eq}$$
$$x = 0 \quad \text{for } x_{eq} < x_d \tag{1}$$

where the quality at the PNVG x_d is calculated by Saha–Zuber's correlation.

For the CHF condition indicated in Fig. 2 ($q_{CHF} =$ 0.9 MW/m^2), Katto's model gave the void fraction to be

Table 1
Experimental conditions for the existing x_d models

Author	G (kg/(m^2 s))	q (MW/m^2)	P (MPa)
Levy [7]	132–1220	0.24–1.91	0.42–14.0
Saha and Zuber [8]	400–1050	0.28–1.89	0.1–13.8
Bowring [17]	0.4–2.0 m/s	0.05–1.90	1.1–14.0
Present Experiment [15]	240–2000	0.35–1.75	0.1

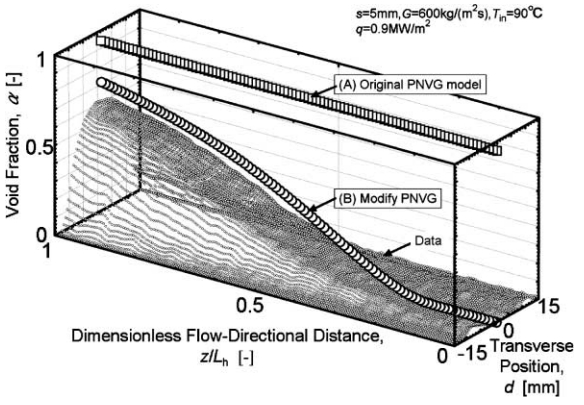

Fig. 13. Void fraction distributions in the Katto CHF model.

0.9 or higher even at the inlet (see (□) calculation result (A) in Fig. 13). As this result physically wrongs, Saha–Zuber's correlation is inadequate to predict the PNVG under the present conditions. If one uses $x_d = -0.0165$ to predict the PNVG in Katto's model, the prediction was much improved to give a proper void fraction distribution and the void fraction at the exit to be about 0.2 (see (◯) calculation result (B) in Fig. 13). The over-estimation of the void fraction by Katto's model would be attributed to the homogeneous equilibrium mixture model which does not take account of the effects of subcooled void and relative velocity between phases. The method of calculation for void fraction at the downstream of the PNVG should also be discussed in a future study. If one uses measured value of $x_d = -0.0165$ in Katto's model, the accuracy of CHF prediction is improved significantly, which method we call here modified Katto' model. Fig. 14 compares the CHF predictions by original Katto's model (◯) and by modified Katto's model (▲) for the existing database [5] for a rectangular channel heated from one side. The reason why original model overestimates the CHF around the results by arrow in Fig. 14 is also attributed to the inappropriate

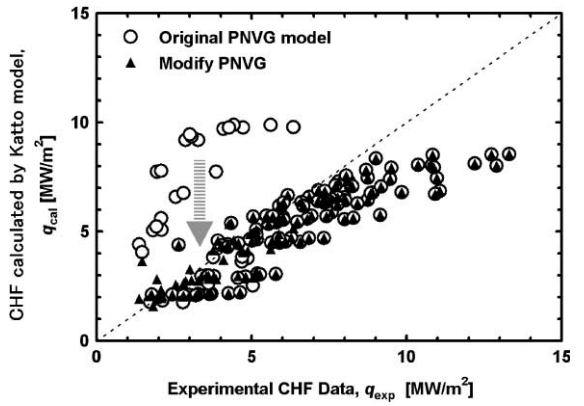

Fig. 14. Effect of PNVG on CHF (Katto CHF model).

prediction of the PNVG. In Fig. 14, some data points of (◯) and (▲) were overlapped. This was attributed to Eq. (1) used in Katto's model. For those cases of the overlapped (◯) and (▲), both the flow rate and the heat flux were so high that the quality at CHF location was very low. Then, the condition for Eq. (1) becomes $x_{eq} < x_d$ and Eq. (1) yields the true quality at CHF location and consequently the void fraction to be zero. As a result, both original and modified Katto's models gave same results with $C/E = 0.5 \sim 1.2$. On the other hand, around the CHF conditions indicated by arrow in Fig. 14, the condition at CHF was that $x_d < x_{eq}$ and original Katto's model with Saha–Zuber's correlation for x_d overestimated the CHF with $C/E \cong 0.5 \sim 3$, while modified Katto's model improved the CHF prediction accuracy from $C/E \cong 0.5 \sim 3$ to $C/E \cong 0.5 \sim 1.2$. This result indicates that the equilibrium quality at the PNVG due to a start of remarkable increase in the void fraction, instead of bubble detachment, should be used in calculating CHF by Katto's model. This is not inconsistent with the observation that tiny bubbles migrated under the actual CHF conditions [5]. Under such a condition, the true quality, and so the void fraction, should be $x \neq 0$ and $\alpha \neq 0$. In Katto's model, however, the true quality x was calculated to be 0 when $x_{eq} < x_d$. At this moment, there is no suitable model available that can calculate the void fraction in such a very low void fraction region. Prediction of very low void fraction under very high heat flux conditions should be one of important future subjects in relation to forced convection subcooled boiling CHF.

5. Conclusions

The void fraction in a rectangular channel with a short heated length was measured by HFR-NR. The PNVG was determined from the obtained void fraction data. The following results were obtained:

(1) From the comparison between the instantaneous PNVG and the time-averaged PNVG, the thermal equilibrium quality at the instantaneous PNVG varied in the range within ± 0.002 from the thermal equilibrium quality at the time-averaged PNVG.
(2) Effects of the heat flux, channel gap, mass velocity, and inlet water temperature on the thermal equilibrium quality at the time-averaged PNVG were small.
(3) From the comparison of the existing PNVG correlations and the measured values, the correlations tended to underestimate the thermal equilibrium quality at the PNVG.
(4) By replacing the equilibrium quality at the PNVG calculated by Saha–Zuber correlation in Katto's CHF model by the measured equilibrium quality at the PNVG, the prediction accuracy of modified

Katto's model was much improved from $C/E \cong 0.5 \sim 3$ to $C/E \cong 0.5 \sim 1.2$, where C/E indicates the ratio of prediction to experimental values.

References

[1] M. Kureta, K. Mishima, H. Nishihara, Critical heat flux for flow-boiling of water in small-diameter tubes under low-pressure conditions, Trans. JSME B 61 (1995) 4109–4116, in Japanese.

[2] G.P. Celata, M. Cumo, A. Mariani, M. Simoncini, G. Zummo, Rationalization of existing mechanistic models for the prediction of water subcooled flow boiling critical heat flux, Int. J. Heat Mass Transfer 37 (1994) 347–360.

[3] Y. Sudo, M. Kaminaga, Critical heat flux at high velocity channel flow with high subcooling, Nucl. Eng. Des. 187 (1999) 215–227.

[4] G.P. Celata, M. Cumo, Y. Katto, A. Mariani, Prediction of the critical heat flux in water subcooled flow boiling using a new mechanistic approach, Int. J. Heat Mass Transfer 42 (1999) 1457–1466.

[5] M. Kureta, H. Akimoto, Experimental study on critical heat flux along one-side heated rectangular channel under subcooled conditions, in: Proc. of ICONE-6, California, USA, 1998, p. 6226.

[6] M. Kureta, H. Akimoto, Critical heat flux of subcooled flow boiling in narrow rectangular channels, in: Proc. of ICONE-7, Tokyo, Japan, 1999, p. 7017.

[7] S. Levy, Forced convection subcooled boiling prediction of vapor volumetric fraction, Int. J. Heat Mass Transfer 10 (1967) 951–965.

[8] P. Saha, N. Zuber, Point of net vapor generation and vapor void fraction in subcooled boiling, in: Proc. of the 5th Int. Heat Transfer Conf. Tokyo, Japan, vol. 4, 1974, pp. 175–179.

[9] E.L. Bibeau, M. Salcudean, A study of bubble ebullition in forced-convective subcooled nucleate boiling at low pressure, Int. J. Heat Mass Transfer 37 (1994) 2245–2259.

[10] G.E. Dix, Vapor void fractions for forced convection with subcooled boiling at low flow rates, NEDO-10491, General Electric Co, 1971.

[11] R.A. Egen, D.A. Dingee, J.W. Chastain, Vapor formation and behavior in boiling heat transfer, BMI-1163, 1957.

[12] G.W. Maurer, A method of predicting steady-state boiling vapor fractions in reactor coolant channels, WAPD-BT–19, 1960.

[13] F.W. Staub et al., Heat transfer and hydraulics—the effects of subcooled voids, Final report, NYO-3679-8, 1969.

[14] R. Martin, Measurement of the local void fraction at high pressure in a heating channel, Nucl. Sci. Eng. 48 (1972) 125–137.

[15] M. Kureta, H. Akimoto, T. Hibiki, K. Mishima, Void fraction measurement in subcooled-boiling flow using high-frame-rate neutron radiography, Trans. ANS. Nucl. Technol. 136 (2001) 241–254.

[16] A. Ohnuki, H. Kamo, H. Akimoto, Development of multidimensional two-fluid model code ACE-3D for evaluation of constitutive equations, JAERI-Data/Code 96-033, 1996 (in Japanese).

[17] R.W. Bowring, Physical model based on bubble detachment and calculations of steam voidage in the subcooled region of a Heated Channel, HPR10, OECD Halden Reactor Project, 1962.

[18] Y. Katto, A prediction model of subcooled water flow boiling CHF for pressure in the range 0.1–20 MPa, Int. J. Heat Mass Transfer 35 (1992) 1115–1123.